DOI: 10.1111/j.1467-8659.2011.02066.x

COMPUTER GRAPHICS *forum*
Volume 30 (2011), number 8 pp. 2354–2366

Visualisation Techniques for Using Spatial Augmented Reality in the Design Process of a Car

Christoffer Menk[1], Eduard Jundt[1] and Reinhard Koch[2]

[1]Volkswagen Group Research, Wolfsburg, Germany
{christoffer.menk, eduard.jundt}@volkswagen.de
[2]Institute of Computer Science, Christian-Albrechts-University of Kiel, Germany
rk@mip.informatik.uni-kiel.de

Abstract

If spatial augmented reality is used in the design process of a car, then one of the most important issues is that the virtual content is projected with a very high visual quality onto the real object, because based on this projection design decisions are made. Especially, the visualised colours on the real object should not be distinguishable from corresponding real reference colours. In this paper, we introduce a new approach for the augmentation of real objects which is able to match the requirements of a design process. We present a new rendering method with ray tracing which increases the visual quality of the projection images in comparison to existing methods. The desired values of these images have further to be adjusted according to the material, the ambient light and the local orientation of the projector. For this purpose, we develop a physically based computation which exactly determines the corresponding projection intensities for these values by using three-dimensional lookup tables at every projector pixel. Since not all of the desired values can be represented with an intensity of the projector, an adjustment has to be computed for these values. Therefore, we conduct a user study with design experts who work in the automotive industry and use the results to propose a new adjustment method for such values. Finally, we compare our methods to existing procedures and conclude which ones are suitable for the design process of a car.

Keywords: virtual and augmented reality, ray tracing, radiometric compensation, projector-camera-systems

ACM CCS: I.3.3 [Computer Graphics]: Picture/Image Generation—I.4.8 [Image Processing and Computer Vision]: Scene Analysis—I.4.9 [Image Processing and Computer Vision]: Applications.

1. Introduction

The automotive industry uses a lot of virtual content for designing, developing and assessing new components of a car. This virtual content is traditionally visualised by using a monitor, projection wall or CAVE. However, real objects, e.g. hardware mockups, are still used and preferred in most steps of the design process, because the designer has a more realistic assessment of the components in reality. Therefore, spatial augmented reality is interesting for such a process, because it is a technique, where projectors are used to visualise the virtual content directly on the real object. Thus, the number of required hardware mockups as well as the number of design iterations could significantly be reduced by using one basic real object and projected virtual contents. In such a scenario, the virtual content represents different colours, variants or arrangements of components and has only small geometric deviations to the geometry of the real object. Therefore, a tracking of the designer is not absolutely necessary, but it is even more important that the content is presented with a high visual quality. Especially, the colours appearing on the real object should be realistic, because based on this projection design decisions are made. For this purpose, it is necessary to account for the ambient light, the material, the colour model and the local orientation of the projector. We address all these issues by applying a new method which uses a physically-based computation with ray tracing. This method is able to achieve a visual quality which is sufficient for the design process (Figure 1).

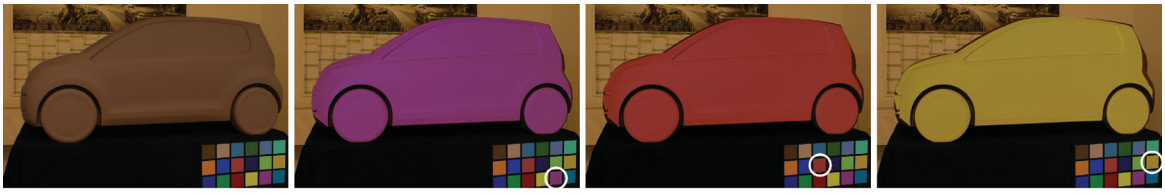

(a) (b) (c) (d)

Figure 1: *Images taken with a real camera from a brown real object (a) which is augmented with a projector: (b,c,d) Our physically-based method is used to visualise one uniform colour on the brown real object. The projected colour is not distinguishable from the corresponding real reference colour which is marked with a white circle.*

1.1. Related work

Raskar *et al*. [RWLB01] presented the idea of shader lamps, where projectors are used to project additional graphical content onto a real object. There are two main issues for spatial augmented reality applications: (1) A projection image of the virtual content has to be created which is seen undistorted by an observer, when it is projected onto the real object. (2) This projection image has further to be radiometrically compensated according to the surface reflectance, the ambient light, the illumination of the projector and of course the perception of the observer.

***Generation of projection images*:** The projection images can be created with a two-pass rendering approach using projective textures which was introduced by Raskar *et al*. [RWC*98]. The projective textures step of the two-pass rendering approach can be replaced with an image warping. In this case, a camera is placed in the viewing position of the observer. The information for the warping is determined by a detection of the projector pixels with structured light techniques. This approach was used in applications where the geometry of the scene is unknown [NPGN03, GPNB04, BEK05]. A distributed rendering system, which is able to compute the projection images for multiple projectors and moving projection surfaces, was presented in [YSN*10]

All described approaches can be applied in real-time, but are likely to produce visible artefacts, because the pixels of the observer image and that of the projection image have different and varying sampling rates on the real object (Figures 2(a–c)). These artefacts can be minimised to some degree by choosing a higher resolution of the observer image (Figure 2(d)) or if the projection surface is flat, by selecting an optimal viewing position (Steele *et al*. [SJY08]).

***Radiometric compensation*:** Raskar *et al*. [RWLB01] considered the reflectance of a neutral surface and the local orientation of the projector to the real object, but no ambient light or colour adjustment was taken into account. Nayar *et al*. [NPGN03] projected onto arbitrary flat surfaces by using a radiometric model which minimises the effects of the surface imperfections. The colour mixing between each projector and corresponding camera pixel was described with a 3×3 colour mixing matrix. This matrix can be represented unnormalised and expanded with a fourth row to account for the ambient light [YHS03]. The radiometric model was enhanced by Grossberg *et al*. [GPNB04] by using the fact that the non-linear projector response is the same for all projector pixels. The described techniques create clipping artefacts if a value is out of the projection range [BIWG08] and additionally, no indirect illumination between the projector pixels was considered. One way to extend the range of projectable values is to use multiple projectors as proposed by Bimber *et al*. [BEK05] or a transparent film [BCK*05].

Other techniques consider besides the projection surface also the content for the radiometric compensation of the projection image. Wang *et al*. [WSOS05] applied an error metric according to the human perception to compensate gray

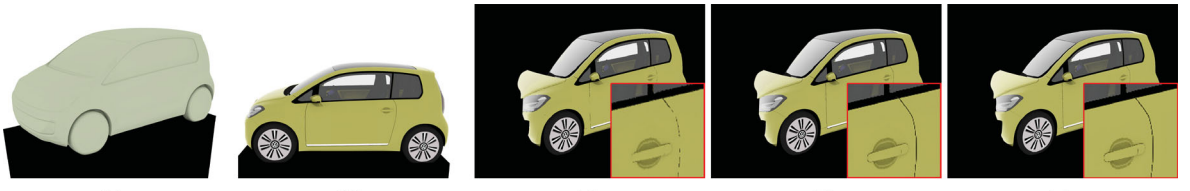

(a) (b) (c) (d) (e)

Figure 2: *(a) Viewing position of projector: Real object which should be augmented with graphical content; (b) Observer image with the desired virtual content which is used to produce the projection image; Projection image which is computed with the two-pass rendering approach from an observer image with (c) the same resolution as the projector and (d) a four times higher resolution than that of the projector; (e) Projection image computed with our approach using the projector resolution.*

projection images. A more complex photometric adaptation was proposed by Ashdown *et al*. [AOSS06], where a luminance and chrominance fitting was applied according to certain specified properties. Their work considers both, a radiometric model of the system and the content of the image, but is not applicable to real-time applications. A radiometric compensation technique which preserves a maximum of luminance and contrast and runs in real-time was proposed in [GB08].

Wetzstein and Bimber [WB07] proposed a technique which additionally considers the global illumination by computing the full light transport between projector and camera. They used a global scaling factor which was derived from the average luminance of the projection image. Light transport matrices between multiple projectors and a camera and an energy minimisation method were also applied to change the physical appearance of deteriorated objects [ALY08]. The light transport was captured in both applications with the technique proposed by Sen *et al*. [SCG*05]. The drawback is that it takes several hours to capture all information. Sheng *et al*.[SYC10] presented a method which interactively minimises the difference between the desired and actual illumination for a setup with multiple projectors, but no ambient light or colour model of the projectors was considered.

The described techniques store the relation between projection intensities and resulting colours on the real object in two captured images or in a colour mixing matrix for every single pixel. These approaches are not accurate enough for colour critical applications. Therefore, traditional colour profiling techniques are able to replace this matrix with a complex three-dimensional lookup table (3D LUT) for the characterisation of monitors [KHM10] or projectors which display content onto a planar screen [TCH*08]. For these traditional displays, it is sufficient to measure the 3D LUT for a limited number of pixels over the monitor or screen and to interpolate the 3D LUT for all other pixels.

This procedure is not applicable to our scenario, because the projector displays the content onto a complex real object and therefore, a 3D LUT would have to be captured for every single projector pixel. This would be time-consuming and would require a lot of memory, especially if spectral values are used. Furthermore, the captured information contains for both of the techniques, namely 3D LUT and colour mixing matrix, the surface reflectance, the colour and depending on the technique also the ambient light. The information has thus to be recaptured, if the position of the projector or the real object is exchanged.

1.2. Main contributions and overview

We describe in Section 2, a technique for the generation of projection images with ray tracing which directly creates the necessary information for every pixel of the projection image (Figure 2(e)) and therefore, does not create the described visual artefacts (Section 1.1).

Instead of measuring the 3D LUTs for every single pixel, we measure a 3D LUT once for one single pixel and use a physically based computation to determine the individual 3D LUTs for every other projector pixel (Section 3). Our approach has the advantage that real objects can be easily exchanged and the projector can be moved without measuring the 3D LUT of the projector again. Furthermore, it achieves a high accuracy so that projected colours are not distinguishable from real reference colours (Figure 1).

The visualisation of real reference colours on the real object is only possible, if they are inside the gamut of each projector pixel. Colours out of range have to be mapped into the corresponding gamut (Section 3.2.2). In our scenario, the gamut of each projector pixel varies over the complete real object due to the different influences of ambient light, real object and projector. Furthermore, the projected content is seen by an observer under these influences in contrary to a presentation on a traditional display. To account for these influences, we conduct a user study where design experts are asked to adjust colours and use the results to create a new adjustment method (Section 3.3). This method is, in contrast to the methods in [AOSS06, GB08], scalable so that it is able to meet the individual preferences of every designer. Finally, a second user study is performed to evaluate which methods are suitable for the design process of a car (Section 4).

2. Generation of projection images

For the rendering techniques, which are described in this section, the geometric relationships between the projector, the real object and the observer have to be known. For this purpose, we determine the intrinsic parameters of the projector as described in [MK10]. The calibrated projector is geometrically registered to the real object by shifting a cross-hair to known 3D coordinates [RWLB01]. These correspondences between 2D and 3D coordinates are used to compute the pose of the projector to the real object. The viewing position of the observer is defined for automotive scenarios, but could also be tracked with an optical measurement system. There are also other geometric registration techniques, but since this is a well-discussed topic in research, we do not further describe it in this paper and the interested reader is referred to [BIWG08]. An evaluation of geometric registration methods can be found in [MJK10].

The information of the geometric registration is used to create a projection image of the virtual content which appears undistorted to the observer, when it is projected onto the real object. Such a projection image can be created from an observer image by using the two-pass rendering approach with projective textures. The approach is sketched in Figure 3(a) and can lead to visible artefacts in the projection image as mentioned in Section 1.1. The problem is that the

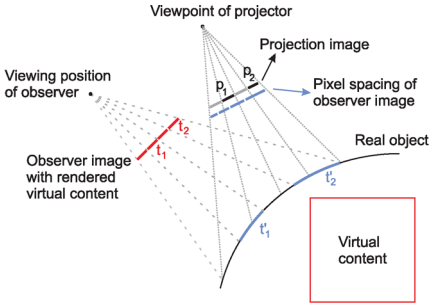

(a) Two-pass rendering with projective textures

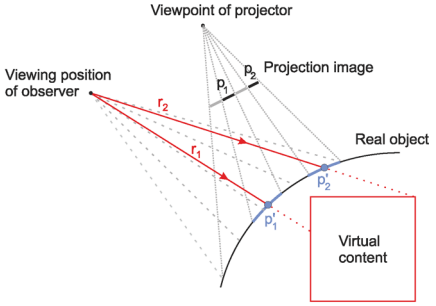

(b) Rendering approach with ray tracing

Figure 3: *Principle of generating a projection image.*

information for a projector pixel like p_1 has to be interpolated from the corresponding pixels of the observer image. The quality of the projection can be increased by choosing a higher resolution for the observer image.

2.1. Rendering approach with ray tracing

Our new approach is sketched in Figure 3(b) for two projector pixels p_1 and p_2. We trace for every projector pixel the ray towards the real object and compute the intersections with the projection surface at p'_1 and p'_2. Then, the rays from the observer viewing position towards the intersections are derived. The ray tracing process is started with rays like r_2 on the virtual content. Note that also a super-sampling for the complete area of the intersections at p'_2 can be performed and used to compute the value for the corresponding projector pixel p_2. An advantage is that our approach does not need an observer image and that the ray tracing is done for every projector pixel so that no unnecessary information is computed. Our approach leads to equal sampling rates on the real object for the observer and projection image and therefore, achieves a higher visual quality than the two-pass rendering approach with projective textures.

A big advantage of the two-pass rendering approach without ray tracing is that it can be used in real-time, but in the design process of a car the visual quality is more important. The visual quality is not only increased by generating the projection image with our proposed method, but also by using ray tracing to account for global illumination effects like reflections which are important for automotive applications. Since automotive applications use ray tracing to create such high quality images, our approach can easily be integrated into existing software.

3. Radiometric compensation

We use a physically-based rendering software and thus, the projection image, whose creation was described in the previous section, consists of radiance values L. These values describe the desired radiance on the surface of the real object. Therefore, the local orientation of the projector to the real object, the ambient light, the material of the real object and the colour model of the projector have to be considered to create projection intensities which result in the desired radiance values L on the real object.

3.1. Material and ambient light

In this paper, we consider two real objects with different materials which are shown in Figures 1(a) and 4(a) as a projection surface. These real objects are used in a design process of a car and are made of a gray or brown diffuse material. The spectral reflectance of the surface is determined by taking measurements on different positions on the surface of the real objects with a spectrophotometer. The average of these measurements is used as the overall surface reflectance.

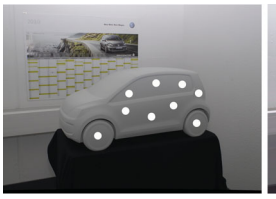

(a) Photograph of real scene

(b) Rendering

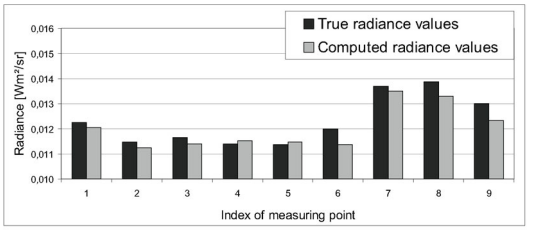

(c) Comparison between true and rendered radiance values

Figure 4: *(a) Image captured with a real camera and (b) physically-based rendering of the real object, which is placed on a black box; (c) Comparison between measured and rendered radiance values on nine positions on the real object which are marked with a white circle in (a).*

The ambient light is measured and integrated into the computation as proposed in [MK10]: A high dynamic range (HDR) map is taken of the surrounding environment and is scaled to match the true radiance values of the scene. The scaling factor is determined by taking measurements of the environment with a spectroradiometer. Finally, the captured environment is mapped onto the room geometry and is used as a light source in our rendering.

This method allows us to compute renderings which consist of the ambient light values on the real object for arbitrary projector or observer positions. An example for a rendering of the real object compared to the real scene is shown in Figure 4. The comparison between measured and rendered radiance values shows that there are only small and neglectable differences between reality and computation. Similar results are obtained with the brown real object.

3.2. Computation of projection values

The relation between radiance values on the real object and projection intensities is described in our approach by using a 3D LUT for every single projector pixel. This table is built from measurements of intensity combinations of the different channels. Previous works did not consider such a complex model, because the storage of such a table for every single pixel would require a lot of memory, e.g. using a $12 \times 12 \times 12$ grid, a resolution of 1400×1050 pixels and a precision of 16-bit, would require 5.1 GB. Our idea is to use a physically-based computation and thus, it is sufficient that the 3D LUT is only stored for one pixel (3.3 MB), because the 3D LUTs for all other pixel of the projector are computed by incorporating the material, the ambient light and the local orientation of the projector. This idea is sketched in Figure 5 and is explained in this section.

The projector, whose intrinsic parameters are calibrated in advance, is geometrically registered to the real object. Then, a spectroradiometer is used to measure the spectrum $L_v(p, I, \lambda)$ of different projection intensities $I = (R, G, B)$ at a specific projector pixel p for wavelengths λ from 380 to 780 nm with a step size of 1 nm (Figure 5, step 1). The projection intensities I are created by dividing the RGB intensity axes into arbitrary steps. The influences of different step sizes are evaluated in Section 4. We use the estimated pose of the projector and the geometry of the real object to transform the measurements $L_v(p, I, \lambda)$ from the measuring position to the projection centre which results in the values $L_c(I, \lambda)$ (Figure 5, step 2). This is shown in Eq. 1, where $\vec{n}_p$ denotes the normal of the surface at pixel p, $\vec{r}_p$ is the normalised vector from pixel p towards the real object with distance d_p and $m(p, \lambda)$ is the reflectance of the diffuse material for a specific wavelength λ.

$$L_c(I, \lambda) = \frac{L_v(p, I, \lambda)\, \pi\, d_p^2}{\left(-\vec{r}_p^{\,T}\, \vec{n}_p\right)\, m(p, \lambda)} \tag{1}$$

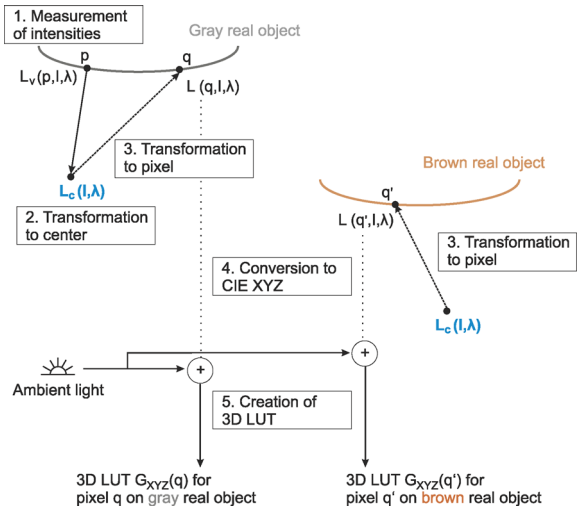

Figure 5: *Idea of using a physically-based computation to determine the projectable radiance values. The derived values $L_c(I, \lambda)$ can also be used to compute the projectable values on the brown real object.*

Note that the measurements are taken without ambient light. Otherwise, an additional measurement of the ambient light spectrum has to be taken and subtracted from $L_v(p, I, \lambda)$. The values of the ambient light which were computed in Section 3.1 cannot be used for this purpose, because they are represented in a 3D colour space. It is very important that the derived values $L_c(I, \lambda)$ are independent of the material, the ambient light and the local orientation of the projector whereas the orientation is represented by the distance d_p and the ray $\vec{r}_p$ towards the pixel p on the real object. Therefore, the derived values can be used in a scenario where the real object is exchanged, the projector changes position or different ambient light is used without measuring the projection intensities again. This is sketched in Figure 5, where the values $L_c(I, \lambda)$ are also used to compute the projectable spectrum at arbitrary pixels on the brown real object. For this purpose, Eq. 1 is extended to compute the resulting spectrum $L(q, I, \lambda)$ of an intensity I at an arbitrary pixel q which is shown in Eqs. 2 and 3.

$$L(q, I, \lambda) = \frac{L_c(I, \lambda)\, \left(-\vec{r}_q^{\,T}\, \vec{n}_q\right)\, m(q, \lambda)}{\pi\, d_q^2} \tag{2}$$

$$L(q, I, \lambda) = L_v(p, I, \lambda) \frac{\left(-\vec{r}_q^{\,T}\, \vec{n}_q\right) m(q, \lambda)\, d_p^2}{\left(-\vec{r}_p^{\,T}\, \vec{n}_p\right)\, m(p, \lambda)\, d_q^2} \tag{3}$$

The values $L(q, I, \lambda)$ for an arbitrary pixel q should be directly computed by using Eq. 3. If Eqs. 1 and 2 is applied one after another, then this will lead to numerical problems,

Table 1: *Deviation between measured and computed radiance values if Eq. 3 is used with spectral or XYZ values: The $L_v(p, I, \lambda)$ values are measured on the gray real object for intensities $I = (R, G, B)$ with $R, G, B \in \{0, 50, \ldots, 200, 255\}$ and used to compute the corresponding values $L(q, I, \lambda)$ on the brown real object.*

	Spectral	CIE XYZ
Average	0.002 [Wm^2/sr] ($\Delta E^* = 0.6$)	0.008 [Wm^2/sr] ($\Delta E^* = 4.9$)
Maximum	0.004 [Wm^2/sr] ($\Delta E^* = 1.3$)	0.015 [Wm^2/sr] ($\Delta E^* = 8.8$)

because the values for $L_c(I, \lambda)$ will get very large. We are trying to use spectral values as long as possible to achieve a higher accuracy. This is also the reason why we do not use a calibrated HDR camera to take the measurements. The difference between a computation of Eq. 3 with spectral versus CIE XYZ values is shown in Table 1. Note that there is no deviation between these computations if the materials $m(p, \lambda)$ and $m(q, \lambda)$ would be equal, because the other factors are equal for all wavelengths.

So far, we have computed the projectable spectrum for different intensities at specific positions on the real object (Figure 5, step 3). These values are now converted into the CIE XYZ space, because the values of the desired result and the ambient light are not in the spectral domain (Figure 5, step 4). Since the projectable values also depend on the present ambient light, this light has to be added (Eq. 4). The ambient light was computed in Section 3.1 and $\overline{x}$, $\overline{y}$ and $\overline{z}$ are the CIE standard observer functions.

$$\begin{aligned} X(q, I) &= \int_\lambda \overline{x}(\lambda) L(q, I, \lambda) d\lambda + X_{amb}(q) \\ Y(q, I) &= \int_\lambda \overline{y}(\lambda) L(q, I, \lambda) d\lambda + Y_{amb}(q) \\ Z(q, I) &= \int_\lambda \overline{z}(\lambda) L(q, I, \lambda) d\lambda + Z_{amb}(q) \end{aligned} \tag{4}$$

The computed values $(X(q, I), Y(q, I), Z(q, I))$ for the projected intensities I represent a 3D grid of XYZ values for every projector pixel q on the real object. These grids are different for every pixel q and represent the gamut. We denote these grids as $G_{XYZ}(q)$ (Figure 5, step 5). Additionally, we have for every projector pixel a desired value $XYZ_{des}(q) = (X_{des}(q), Y_{des}(q), Z_{des}(q))$, which was created during the rendering of the projection image as described in Section 2.1. Such a desired value does not need necessarily to be represented by an intensity of the projector, because the projectable values depend on the ambient light, material and local orientation of the projector. Therefore, the next sections describe how an intensity can be found which is a good choice for the representation of the desired value.

3.2.1. *Handling values inside the gamut*

If a desired value $XYZ_{des}(q)$ for a pixel q is inside the gamut, then it is included by the computed 3D grid $G_{XYZ}(q)$. The coordinates of the value inside this grid can be determined by using tetrahedral division and barycentric coordinates [Hun92]. The tetrahedral division is applied to the 3D grid $G_{XYZ}(q)$ of XYZ values $(X(q, I), Y(q, I), Z(q, I))$, which describe the projectable values for a specific pixel q. Note that every point of this grid corresponds to a certain projection intensity $I = (R, G, B)$ and a tetrahedron of this grid is formed by four values $(X(q, I_i), Y(q, I_i), Z(q, I_i))$ with $i \in \{0, 1, 2, 3\}$. The barycentric coordinates α, β and γ of a desired value $XYZ_{des}(q)$ corresponding to a tetrahedron can be computed by using Eq. 5, where $X_i = X(q, I_i)$, $Y_i = Y(q, I_i)$ and $Z_i = Z(q, I_i)$.

$$\begin{pmatrix} \alpha \\ \beta \\ \gamma \end{pmatrix} = M_{XYZ}^{-1} \begin{pmatrix} X_{des}(q) - X_0 \\ Y_{des}(q) - Y_0 \\ Z_{des}(q) - Z_0 \end{pmatrix} \tag{5}$$

$$M_{XYZ} = \begin{pmatrix} X_1 - X_0 & X_2 - X_0 & X_3 - X_0 \\ Y_1 - Y_0 & Y_2 - Y_0 & Y_3 - Y_0 \\ Z_1 - Z_0 & Z_2 - Z_0 & Z_3 - Z_0 \end{pmatrix} \tag{6}$$

If the barycentric coordinates α, β and γ are inside [0, 1] and $\alpha + \beta + \gamma \leqslant 1$, then the desired colour value is inside the tetrahedron and Eq. 7 can be used to determine the final intensity $I_{des}(q) = (R_{des}(q), G_{des}(q), B_{des}(q))$.

$$I_{des}(q) = M_{RGB} \begin{pmatrix} \alpha \\ \beta \\ \gamma \end{pmatrix} + \begin{pmatrix} R_0 \\ G_0 \\ B_0 \end{pmatrix} \tag{7}$$

$$M_{RGB} = \begin{pmatrix} R_1 - R_0 & R_2 - R_0 & R_3 - R_0 \\ G_1 - G_0 & G_2 - G_0 & G_3 - G_0 \\ B_1 - B_0 & B_2 - B_0 & B_3 - B_0 \end{pmatrix} \tag{8}$$

Since it is very time-consuming to compute the barycentric coordinates for all created tetrahedrons, we implemented a bounding box approach so that not all tetrahedrons have to be tested for an inclusion of the desired value. Note that the interpolation between the measurements is an approximation, because the projection values are non-linearly related. The error caused by this approximation gets smaller as more measurements are made which results in a finer resolution of the grid $G_{XYZ}(q)$ for a pixel q. Instead, the relation of the projection intensities could also be made more linear by optimising the grid structure [TCH*08] or by using a gamma correction for each colour channel.

3.2.2. *Handling values outside the gamut*

There are several intents of handling colours outside the gamut which are known from traditional displays. For our

scenario, we consider in a first step the relative colorimetric rendering intent which maintains the exact relationship between colours inside the gamut while colours outside the gamut are clipped. This intent is adapted for our scenario with two methods which describe the mapping of colours outside the gamut while values inside the gamut are computed with the 3D LUT method as described in the previous section.

$\Delta E^* -$ Min: The idea behind this approach is very simple: Values which are outside the gamut are visualised by choosing a projectable value which has the smallest ΔE^* distance. For this purpose, the grid, representing the gamut of the corresponding projector pixel, is converted to the CIE LAB colour space which results in the values $LAB(q, I) = (L^*(q, I), a^*(q, I), b^*(q, I))$, where (L^*, a^*, b^*) are the coordinates of the CIE LAB colour space. The desired colour value $XYZ_{des}(q)$ is also transformed to this colour space and is denoted as $LAB_{des}(q) = (L^*_{des}(q), a^*_{des}(q), b^*_{des}(q))$. The CIE LAB colour space has the advantage that it is perceptually uniform. Thus, the Euclidean distances ΔE^* between different values in this colour space are equally perceived by an observer. We want to find the projection intensity which has the smallest distance to the desired value $LAB_{des}(q)$. This is described in Eq. 9.

$$\min_I \Delta E^*(q, I) = \min_I \|LAB(q, I) - LAB_{des}(q)\|_2 \quad (9)$$

A simple approach would be to create the projection values for all discrete intensities I by interpolating between the values of the transformed grid $G_{LAB}(q)$ and to search for the projection value with the smallest ΔE^*. Since the desired value is outside the grid, an elaborate approach is to interpolate the projection values at the boundary of the grid and to determine their distance towards the desired value.

$\Delta E^*_{ab} -$ Min: This approach is very similar to the one described above, but it neglects the lightness $L^*(q, I)$ and only finds an intensity which has the smallest distance in terms of the chromaticity coordinates $a^*(q, I)$ and $b^*(q, I)$ which is described in Eq. 10.

$$\min_I \sqrt{\left(a^*_{des}(q) - a^*(q, I)\right)^2 + \left(b^*_{des}(q) - b^*(q, I)\right)^2} \quad (10)$$

The minimum distance is determined by constructing a ray from the desired value towards the boundary of the corresponding grid $G_{LAB}(q)$ whereas the points on the ray have a varying lightness value, but the same chromaticity coordinates as the desired value. This can lead to a projection image which creates values with good chromaticity coordinates on the real object, but the overall luminance may be different from the desired one.

3.3. First user study

The previous section proposed two of many different possibilities how values outside the gamut could be handled.

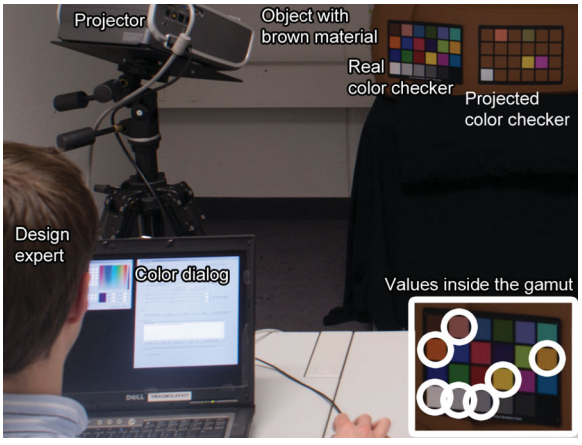

Figure 6: *Setup for our user study. The design experts should replicate the real colour checker by choosing appropriate projection intensities. The colours with a white circle are inside the gamut and are therefore the only colours which can be exactly represented by a projection intensity.*

Therefore, we conduct a user study with 10 design experts, working in the automotive industry, to see how they would adjust such values. Additionally, the methods proposed in the previous section, namely $\Delta E^* -$ Min and $\Delta E^*_{ab} -$ Min, should be evaluated in comparison to the designer's choice. The setup for the experiment is shown in Figure 6: A real colour checker, which tiles are measured with a spectroradiometer, and a ceiling of a colour checker were attached to the brown real object. A projector was used to visualise the computed or selected colours onto the ceiling of the colour checker. The design experts should use a colour dialog to select the most satisfying colour for every tile of the colour checker. The following steps were conducted by every expert:

1. For every tile, the expert should select the most satisfying colour. The current tile for selection was randomly chosen by the program. When all projection intensities for the tiles were selected, the expert had the chance to adjust the overall appearance.
2. In this step, one tile of the colour checker was chosen and three projected colours were randomly shown to the expert: own choice and result from $\Delta E^* -$ Min and $\Delta E^*_{ab} -$ Min. The expert should evaluate all three projected colours with a value from 1 to 7 where 7 means that he is totally satisfied with the visualisation in reference to the corresponding tile of the real colour checker. This step was repeated for all tiles of the colour checker.
3. The overall visualisation of the projected colour checker was rated in this step. The complete three colour checkers ($\Delta E^* -$ Min, $\Delta E^*_{ab} -$ Min and own choice) were projected in random order and the

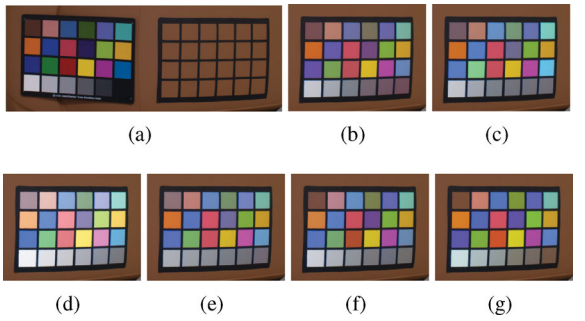

Figure 7: *Images taken with a real camera from: (a) our setup; (b) $\Delta E^* - Min$ which is equal to GLA(0;1;1); (c) $\Delta E^*_{ab} - Min$; (d) GLA(1;0.2;0); (e) GLA(0.15;0;1); (f) Result of first user study from one expert and (g) the average of the results of all experts; The visualisations of the different colour checkers are shown to the design experts in a final user study.*

Table 2: *Average ratings in the user study (step 2). The boldface numbers indicate tiles that are inside the gamut of the corresponding projector pixels and every number corresponds to the average of the ratings for one tile of the projected colour checker (Figure 6). The * indicates if the values are statistically significantly higher than a rating of 5 with $p = 0.05$ and $df = 9$.*

User's choice						
	4.8	***3.6***	3.5	3.0	4.8	4.7
	6.0*	3.2	4.3	2.3	4.2	***5.1***
	2.0	3.0	3.0	***5.4***	4.9	2.9
	4.7	***4.7***	***4.0***	2.5	1.5	1.1
	Computed average of all tiles: 3.7					
$\Delta E^* - Min$						
	5.1	***6.0****	4.3	3.7	5.4	5.1
	5.7*	3.3	5.5*	3.2	5.5*	***5.4****
	2.2	3.8	3.9	***5.8****	4.9	3.3
	6.4*	***6.6****	***6.2****	3.6	1.6	1.1
	Computed average of all tiles: 4.5					
$\Delta E^*_{ab} - Min$						
	3.2	***6.1****	4.0	2.8	5.3	3.5
	5.8*	3.2	5.5*	2.2	5.7*	***5.3****
	1.8	2.4	3.1	***5.5****	5.1	2.2
	6.4*	***6.4****	***6.1****	4.8	2.6	1.3
	Computed average of all tiles: 4.2					

design expert should judge how the overall appearance satisfies him. Examples for these colour checkers are shown in Figures 7(b), (c) and (f) .

4. Step 1. was repeated.

The different ratings of all design experts are presented in Table 2. The boldface ratings illustrate if the corresponding colour is inside the gamut of the corresponding projector pixels. Note that for these colours, the ΔE^*_{ab}- and $\Delta E^* - Min$ methods compute an identical projection intensity, because they both use the 3D LUT method for colours inside the gamut. These colours got a very good rating with a significantly higher value than 5 ($p = 0.05$ and $df = 9$) whereas a rating of 5 can be seen as a minimum acceptable level for a usage in the design process. Therefore, our 3D LUT method is able to visualise colours inside the gamut with an acceptable high quality. The results show further that the 10 design experts gave the best ratings to the $\Delta E^* - Min$ method when only one tile was shown (step 2), which can be seen in the ratings for all single tiles and the computed average value of these ratings in Table 2. This is not surprising, since the ΔE^* metric works in a perceptual space.

Table 3: *Results from rating the overall appearance (step 3).*

User selection	$\Delta E^* - Min$	$\Delta E^*_{ab} - Min$
4.4 ($\sigma = 1.07$)	3.7 ($\sigma = 1.06$)	4.1 ($\sigma = 1.29$)

When the experts rated the overall appearance of the complete projected colour checker (step 3), then the $\Delta E^* - Min$ method got the lowest rating which can be seen in Table 3. However, these overall values cannot be absolutely compared due to their large standard deviation σ, but we noticed that 7 of the 10 design expert gave a higher rating to their own choice compared to $\Delta E^* - Min$. Therefore, we took a look at the values which were selected by the different experts and ask them about their ratings. It was surprising that the chosen colours of the first and fourth step have only small deviations. Furthermore, it could be seen that the experts tried to preserve the chromaticity coordinates of the desired colours. Some of the designers also adjusted colours which are inside the gamut and tried to preserve the relative lightness between the colours and stated that they did not like the visualisation of the blue colours which got too purple with the $\Delta E^* - Min$ method. Thus, the choice of the designers corresponds more to a perceptual colorimetric rendering intent than to a relative one (Section 3.2.2). Therefore, we propose a new method which tries to preserve the chromaticity coordinates of the colours and the relative lightness of the real colour checker. Furthermore, this method is scalable so that each designer can adjust the result to fit his individual preferences. This method is explained in the next section and should get a higher rating for the overall appearance which is further examined in a second user study (Section 4.3).

3.4. Global lightness adjustment (GLA)

We present a scalable method, denoted as global lightness adjustment (GLA), which extends the $\Delta E^* - Min$ method by computing an adjustment for all lightness coordinates of the desired values. After the adjustment, the values

which are out of the projection range are handled with the $\Delta E^* - \text{Min}$ method (Section 3.2.2) and values inside the projection range are computed by using the 3D LUT method (Section 3.2.1). The adjustment can be modulated with three different weights c_1, c_2 and c_3 to match the designer's personal preferences. We abbreviate this method with GLA(c_1; c_2; c_3) in the following sections. The weights are used to compute a global scale factor S_g and a global additive value A_g. Both values are used to adjust the lightness $L^*(q)$ of all pixels q so that the relative lightness between all desired values is preserved. The function used for the adjustment is shown in Eq. 11, where $\overline{L}^*_{des}$ is the average lightness value of all pixels q. In a first step, the minimum $L^*_{\min}(q)$ and maximum lightness values $L^*_{\max}(q)$ for every desired value of a pixel q according to the grid $G_{LAB}(q)$ are determined. This is done by using ray tracing. In a second step, the adjustment is computed by minimising the distance for all pixels q which is shown in Eq. 12.

$$f(q) = \left(L^*_{des}(q) - \overline{L}^*_{des}\right) S_g + \overline{L}^*_{des} + A_g \qquad (11)$$

$$\min_{S_g, A_g} \left\{ \sum_q [c_1\, g(q) + c_2\, |f(q) - A_g| + c_3\, A_g] \right\} \qquad (12)$$

$$g(q) = \begin{cases} 0 & L^*_{\min}(q) \le f(q) \le L^*_{\max}(q) \\ h(q) & \text{otherwise} \end{cases}$$

$$h(q) = \min\{|L^*_{\min}(q) - f(q)|, |L^*_{\max}(q) - f(q)|\}$$

The function $g(q)$ describes the distance from the adjusted value towards the gamut of the projector pixel q. The second and third term compute the distance towards the original values and consider separately the scaling S_g and shifting A_g of the values. These terms can be adjusted by the three weights c_1, c_2, c_3 which can be interpreted as follows: The first weight c_1 determines how important it is that the values are inside the gamut. c_2 denotes how strong the relative lightness between each value should be preserved and the last weight. c_3 determines how important it is that the original values are maintained. These weights can be defined by a designer to account for his personal preferences and we found that these weights are easier to handle than directly choosing the scale factor and additive value. An example for a fitting with different weights can be seen in Figure 8. These weights are also used for our final user study. If weights of $c_1 = 0$, $c_2 = 1$, $c_3 = 1$ are chosen, then the values are not adjusted and this would correspond to the $\Delta E^* - \text{Min}$ method presented in Section 3.2.2. Results from the different approaches which are also used for a final user study are visualised in Figure 7.

4. Results

The experiments are performed with a *Canon Xeed SX6* projector which has a resolution of 1400 × 1050 pixels. The physically-based rendering software RADIANCE [War94] is used as our ray tracer, because it can compute HDR projection images with radiance values. The rendering of the observer image takes 12 and of the ambient light 3 min on two Intel Xeon *X*5570 processors, but could be improved by using a newer ray tracing software. All other computations are done with MATLAB on a single processor. The radiometric compensation of the created projection images takes about 3 min for the virtual content (Figure 9) and 20 s for the colour checker (Figure 7). The compensation of the colour checker takes less time, because it covers a smaller area of the projection image.

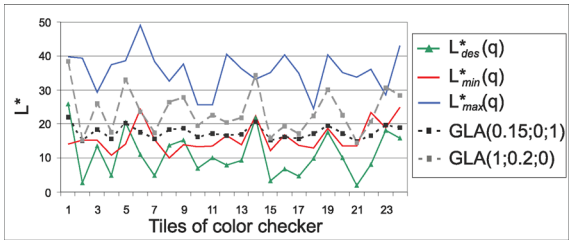

Figure 8: *The lightness values L^* are adjusted with the proposed GLA method for different weights.*

4.1. Generation of projection images

The scenario for our setup is shown in Figure 9(a). The virtual content, which should be projected onto the real object, is rendered under the recorded ambient light to increase the visual appearance. We render for our experiments observer images with a scale factor between 1.0× and 4.0× according to the projector resolution for the two-pass rendering approach and compare the results to our ray tracing method.

The computed projection images are visualised on a real object to see their final appearance and captured with a real camera (Figure 9). The extracted details of the results clearly show that our approach achieves a better visual result than the approach with projective textures if the observer image has the same resolution as the projector (1.0×). The results show that if a 2.0 times higher resolution is used for the observer image that this might not lead to a projection image with a very high quality. An observer image with a 4.0 times higher resolution is necessary to achieve a result equivalent to the result of our ray tracing approach using the projector resolution (1.0×). Furthermore, if we render with our method a projection image with a scale factor of 2.0 which results in a super-sampling, then we will get a visual quality which is not achieved by any scale factor of the projective textures approach. In summary, the results show that there will always be a loss in the visual quality if the two-pass rendering approach is applied, because the information for the projection image is interpolated from the observer image.

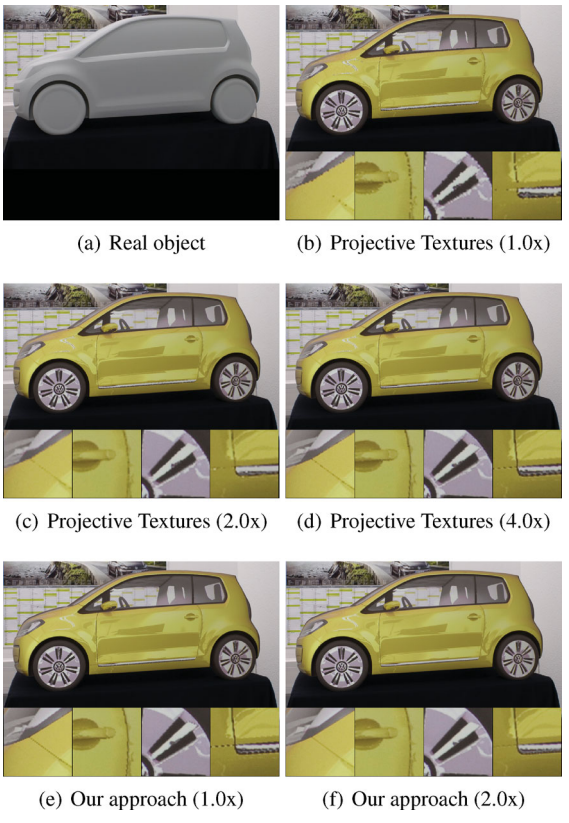

(a) Real object (b) Projective Textures (1.0x)

(c) Projective Textures (2.0x) (d) Projective Textures (4.0x)

(e) Our approach (1.0x) (f) Our approach (2.0x)

Figure 9: *Final results captured with a real camera. The projection images are computed by (b–d) using the two-pass rendering approach with projective textures or (e, f) our new proposed method which uses ray tracing. The resolution is defined with a scale factor according to the projector resolution (1400 × 1050 pixels).*

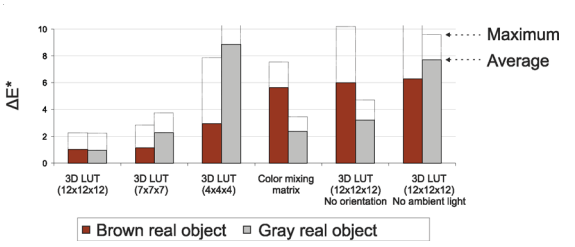

Figure 10: *Measured and averaged accuracy of the different approaches for visualising eight different colours on the two real objects. The measurements are taken on nine different positions on each of the real objects, which results in 72 measurements for each method on the corresponding object.*

4.2. Projection of real colours

This section evaluates the accuracy of our 3D LUT approach to visualise colours which are inside the gamut of the projector and compares it to the method using a colour mixing matrix. The experiment is conducted with both real objects which are shown in Figures 1(a) and 11(a). As described in Section 3.2, the gamut of each projector pixel depends on the material, the ambient light and the local orientation of the projector. Therefore, we determine for every real object eight, randomly selected, CIE XYZ values which are inside the gamut for most of the projector pixels. A big advantage of our method is that a real object can be easily exchanged without measuring the 3D LUT of the projector again. Thus, we measure different projection intensities for one pixel on the brown real object and use our physically based approach to compute the projectable values at all other pixels as well as for all pixels on the gray real object. The projection intensities are determined with two methods: Our proposed 3D LUT method and the method which uses a colour mixing matrix [GPNB04]. The intensities are also computed without the consideration of ambient light or the local orientation of the projector, to examine the influences of these components. Furthermore, we also choose different grid sizes for our 3D LUT method to evaluate their influences on the accuracy.

A spectroradiometer is used to measure the eight chosen CIE *XYZ* values which are inside the gamut of the projector on nine different positions on the real object, which results in 72 measurements for each method on the corresponding object. We use the same positions on the real object which were already used for the comparison of the ambient light [Figure 4(a)]. We compare these measured values to the desired CIE *XYZ* values and are therefore able to give a statement about the accuracy of the different methods. The measured results are presented in Figure 10 and visual results where a real reference colour should be visualised on the complete real object are captured by a camera and shown in Figure 11.

The results clearly show that our approach with a 3D LUT performs very well, since the average ΔE^* value is equal to 1.0 and 0.95 for both models. The projected colours are not distinguishable from each of the eight desired values, because a ΔE^* of 2.3 is denoted as the just noticeable difference [ST97] and also the maximum values are below this threshold. Furthermore, the result shows that the ΔE^* value gets larger as the size of the grid gets smaller. Also the local orientation and ambient light have great influences on the result. Thus, it is necessary that these components are taken into account for the design process of a car. The approach using a colour mixing matrix achieves good results for the gray object with an average value of $\Delta E^* = 2.4$, but on the brown object the average value is with $\Delta E^* = 5.6$ very large. The accuracy of this approach depends on the desired value, since the matrix assumes a linear relationship after gamma correction. The result of the approach using a colour mixing matrix might be good enough to adjust a video, but if the projection should represent real reference colours, then

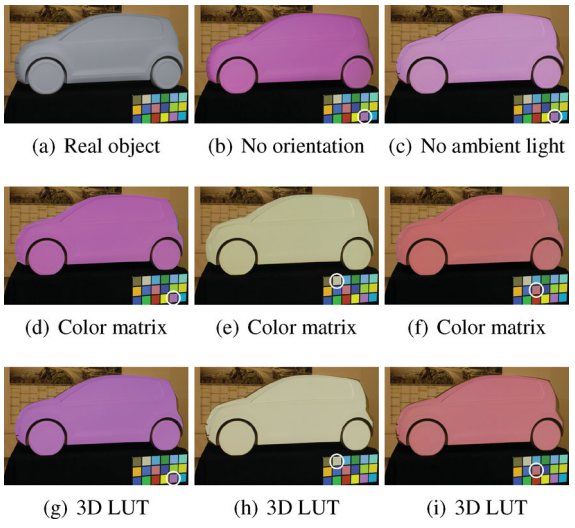

Figure 11: *Images taken with a real camera from the results; (a) Real object which is used in the design process of a car. A colour which is equivalent to a real reference colour (white circle) is projected with different methods onto real object: (b) 3D LUT (12 × 12 × 12) where no local orientation or (c) no ambient light is considered; (d,e,f) Colour mixing matrix; (g, h, i) 3D LUT (12 × 12 × 12) with consideration of all influences. Note that the colour checker is illuminated with a second light source to lift the reference colours into the gamut of the projector. Please zoom in to see more details.*

this method is not sufficient. In summary, it can be seen that our 3D LUT approach with a physically based computation performs very well and can be used for a design process in the automotive industry, because it can accurately represent colours which are inside the gamut.

4.3. Second user study

This user study was conducted two weeks after the first user study (Section 3.3), because the participants should not remember their colour choice and ratings. We conducted this study to see what adjustment methods should be applied to colours out of range and which ones are suitable for the design process of a car. For this purpose, colour checkers which are adjusted with different methods and projected onto the real object are shown to the 10 design experts. Images of these colour checkers can be seen in Figure 7 where Figure 7(f) is always replaced with the colour checker which the expert made in the first user study. The expert should rate how he is satisfied with the result compared to the real colour checker. The rating is a value between 1 and 7, where 7 is the best value. The complete result of this study is shown in Table 4.

If we only consider each method for itself, then the best rating with a value of 4.5 is achieved with the average values

Table 4: *Results from the second user study where the design experts rated the different adjustment methods. The boldface numbers indicate the best result from the three specified weights of the GLA methods.*

Method	GLA(0;1;1) [$\Delta E^* - \text{Min}$]	GLA (0.15;0;1)	GLA (1;0.2;0)	ΔE^*_{ab}-Min	Colors 1. study	Average of user choices
Rating	**7**	3	1	4	6	7
	5	3	4	3	2	5
	5	4	2	3	6	2
	4	**5**	4	2	6	4
	4	**5**	3	2	2	2
	3	5	**6**	3	6	2
	5	3	**6**	3	4	5
	3	3	**5**	2	4	7
	4	3	**5**	4	5	6
	4	2	**5**	4	4	5
Average	4.4	3.6	4.1	3.0	4.5	4.5
Std. dev.	1.2	1.1	1.7	0.8	1.6	2.0

of all colour checkers which were created by the design experts in the first study and the individual choice of every expert. However, some of the experts also give a very low value to their created colour checker from the first user study. In contrary to the first study, the $\Delta E^* - \text{Min}$ method achieves a higher rating, with a value of 4.4, and the $\Delta E^*_{ab} - \text{Min}$ a lower value of 3.0. However, the average values for all of these methods do not give a clue about what method would be the best choice, because they have large standard deviations. This is also the case if we take a look at the overall ratings for different weights of our proposed GLA method. The result shows that every design expert has his own preferences for the adjustment of colours and therefore, one adjustment for all experts is not sufficient. However, it can be seen that at least one of the three tested specifications of weights of the GLA methods gets a rating which is higher than 5. So our proposed method does not always achieves the highest rating, but is able to get a rating which is acceptable with a value of 5 for the design process. Therefore, our method is able to meet the different preferences of the design experts. Since the weights were chosen by us, an evaluation has to be conducted if a higher rating could be achieved when the design experts where able to adjust the weights by themselves.

5. Conclusions and future work

We examined in this paper the use of spatial augmented reality for the design process of a car. For this purpose, we presented a new rendering technique which creates the projection images with ray tracing. This method does not interpolate the values for the projection image and therefore, achieves a higher visual quality than existing approaches. Furthermore, we used a physically-based computation to

determine the projectable values at every projector pixel on the real object by incorporating the ambient light, the material and the local orientation of the projector. The projectable values were represented with a 3D LUT which was computed with our approach for every single projector pixel, since the storage of such a table for every pixel would require too much memory. An advantage of our method is that the real object or the position of the projector can be changed without measuring the colours of the projector again. This is an important issue, because in a design process of a car, a lot of different real objects are illuminated with the same projector and viewed under the same ambient light. Our physically-based 3D LUT method is able to exactly visualise colours, which are inside the gamut of the projector so that they are not distinguishable from a real reference colour. In our experiments, our approach achieves maximum and average ΔE^* values which are below the perceivable threshold of 2.3 and thus, is suitable for a scenario in the automotive industry. Since a lot of colours are outside the gamut of the projector, an adjustment has to be computed. We conducted a user study to see what adjustments a design expert would make. The results were used to propose a new scalable method which preserves the chromaticity coordinates and adjusts the lightness before the corresponding projection intensity is computed. This method performed well in a second user study, because it can be modulated by three weights to meet the designer's personal preferences.

Future work has to evaluate if these weights are suitable for a designer to adjust the overall appearance. Furthermore, our proposed method has to be extended to be applicable to multiple projectors which can enhance the gamut. For this purpose, we are currently implementing our proposed method on the graphics card to increase the performance.

References

[ALY08] Aliaga D. G., Law A. J., Yeung Y. H.: A virtual restoration stage for real-world objects. In *SIGGRAPH Asia '08: ACM SIGGRAPH Asia 2008 papers* (New York, NY, USA, 2008), ACM, pp. 1–10.

[AOSS06] Ashdown M., Okabe T., Sato I., Sato Y.: Robust content-dependent photometric projector compensation. In *CVPRW '06: Proceedings of the 2006 Conference on Computer Vision and Pattern Recognition Workshop* (Washington, DC, USA, 2006), IEEE Computer Society, p. 6.

[BCK*05] Bimber O., Coriand F., Kleppe A., Bruns E., Zollmann S., Langlotz T.: Superimposing pictorial artwork with projected imagery. *IEEE MultiMedia* 12, 1 (2005).

[BEK05] Bimber O., Emmerling A., Klemmer T.: Embedded entertainment with smart projectors. *Computer* 38, 1 (2005), 48–55.

[BIWG08] Bimber O., Iwai D., Wetzstein G., Grundhöfer A.: The visual computing of projector-camera systems. *Comput. Graph. Forum* 27, 8 (2008), 2219–2245.

[GB08] Grundhofer A., Bimber O.: Real-time adaptive radiometric compensation. *IEEE Transactions on Visualization and Computer Graphics 14* (January 2008), 97–108.

[GPNB04] Grossberg M. D., Peri H., Nayar S. K., Belhumeur P. N.: Making one object look like another: Controlling appearance using a projector-camera system. *IEEE Computer Society Conference on Computer Vision and Pattern Recognition 1* (2004), 452–459.

[Hun92] Hung P.-C.: Tetrahedral division technique applied to colorimetric calibration for imaging media. In *Annual Meeting IS and T* (May 1992), pp. 419–422.

[KHM10] Koch J., Henrich N., Müller S.: Spatial color confidence for physically based rendering settings on lc displays. In *GRAPP '10: International Conference on Computer Graphics Theory and Applications* (Angers, France, 2010), Springer.

[MJK10] Menk C., Jundt E., Koch R.: Evaluation of geometric registration methods for using spatial augmented reality in the automotive industry. In *15th International Workshop on Vision, Modeling and Visualization* (Siegen, Germany, 2010).

[MK10] Menk C., Koch R.: Physically-based augmentation of real objects with virtual content under the influence of ambient light. In *Proc. IEEE International Workshop on Projector-Camera Systems* (San Francisco, CA, USA, 2010).

[NPGN03] Nayar S. K., Peri H., Grossberg M. D. N. B. P.: A projection system with radiometric compensation for screen imperfections. In *Proc. of International Workshop on Projector-Camera Systems* (2003).

[RWC*98] Raskar R., Welch G., Cutts M., Lake A., Stesin L., Fuchs H.: The office of the future: a unified approach to image-based modeling and spatially immersive displays. In *SIGGRAPH '98: Proceedings of the 25th annual conference on Computer graphics and interactive techniques* (New York, NY, USA, 1998), ACM, pp. 179–188.

[RWLB01] Raskar R., Welch G., Low K.-L., Bandyopadhyay D.: Shader lamps: Animating real objects with image-based illumination. In *Proceedings of the 12th Eurographics Workshop on Rendering Techniques* (London, UK, 2001), Springer-Verlag, pp. 89–102.

[SCG*05] Sen P., Chen B., Garg G., Marschner S. R., Horowitz M., Levoy M., Lensch H. P. A.: Dual photography. In *ACM SIGGRAPH 2005 Papers* (New York, NY, USA, 2005), ACM, pp. 745–755.

[SJY08] Steele R. M., Jaynes C., Yang R.: Reducing resolution loss in two-pass rendering by optimal view directions and display-surface partitioning. In *PROCAMS '08: Proceedings of the 5th ACM/IEEE International Workshop on Projector camera systems* (New York, NY, USA, 2008), ACM, pp. 1–8.

[ST97] Sharma G., Trussell H. J.: Digital color imaging. *IEEE Transactions on Image Processing 6* (1997), 901–932.

[SYC10] Sheng Y., Yapo T. C., Cutler B.: Global illumination compensation for spatially augmented reality. *Computer Graphics Forum 29* (May 2010), 387–396(10).

[TCH*08] Thomas J.-B., Colantoni P., Hardeberg J. Y., Foucherot I., Gouton P.: An inverse display color characterization model based on an optimized structure. In *Color Imaging XIII: Processing, Hardcopy, and Applications* (San Jose, USA, Jan. 2008), vol. 6807, SPIE.

[War94] Ward G. J.: The radiance lighting simulation and rendering system. In *SIGGRAPH '94: Proceedings of the 21st annual conference on Computer graphics and interactive techniques* (New York, NY, USA, 1994), ACM, pp. 459–472.

[WB07] Wetzstein G., Bimber O.: Radiometric compensation through inverse light transport. In *PG '07: Proceedings of the 15th Pacific Conference on Computer Graphics and Applications* (Washington, DC, USA, 2007), pp. 391–399.

[WSOS05] Wang D., Sato I., Okabe T., Sato Y.: Radiometric compensation in a projector-camera system based properties of human vision system. In *IEEE International Workshop on Projector-Camera Systems* (Washington, DC, USA, 2005), IEEE Computer Society, p. 100.

[YHS03] Yoshida T., Horii C., Sato K.: A virtual color reconstruction system for real heritage with light projection. In *VSMM '03: Proceedings of International Conference on Virtual Systems and Multimedia* (2003), pp. 161–168.

[YSN*10] Yapo T., Sheng Y., Nasman J., Dolce A., Li E., Cutler B.: Dynamic projection environments for immersive visualization. In *Proc. of IEEE International Workshop on Projector-Camera Systems* (2010), pp. 1–8.